JOURNAL OF GEOPHYSICAL RESEARCH, VOL. 114, D07112, doi:10.1029/2008JD011261, 2009

Detection of temperatures conducive to Arctic polar stratospheric clouds using CHAMP and SAC-C radio occultation data

M. de la Torre Juárez,[1] S. Marcus,[1] A. Dörnbrack,[2] T. M. Schrøder,[1,3] R. Kivi,[4] B. A. Iijima,[1] G. A. Hajj,[1] and A. J. Mannucci[1]

Received 7 October 2008; revised 14 December 2008; accepted 11 February 2009; published 15 April 2009.

[1] We use global positioning system radio occultation (GPSRO) data from the Challenging Mini-Satellite Payload for Geophysical Research and Application (CHAMP) and Satélite de Applicaciones Científicas-C (SAC-C) low Earth orbiting satellites to investigate the occurrence of air with temperatures cold enough to allow the formation of polar stratospheric clouds (PSCs) during four successive Arctic winters spanning 2001 to 2005. The GPSRO data are validated and compared with analysis data from the European Centre for Medium-Range Weather Forecasts using a series of criteria designed to eliminate faulty soundings but retain profiles which do not differ too strongly from the model data. We find that GPSRO is able to detect more PSC-prone temperature profiles during winters with disturbed conditions (in particular during December 2001 and 2003) than the analysis, but that the model fully captures the extent of PSC-prone air in winters with strong, cold vortices (in particular December 2002 and January 2005). Examination of detailed profiles for December 2001 shows that this difference is due to the ability of GPSRO to detect short-vertical wavelength features which may represent either localized gravity or global-scale planetary waves. Since the GPSRO data are now being directly assimilated into operational analysis systems, the benefits of the higher vertical resolution retrievals it provides should become evident in future observational studies of PSC formation and ozone loss, particularly under the disturbed conditions noted in several recent winters.

Citation: de la Torre Juárez, M., S. Marcus, A. Dörnbrack, T. M. Schrøder, R. Kivi, B. A. Iijima, G. A. Hajj, and A. J. Mannucci (2009), Detection of temperatures conducive to Arctic polar stratospheric clouds using CHAMP and SAC-C radio occultation data, *J. Geophys. Res.*, *114*, D07112, doi:10.1029/2008JD011261.

1. Introduction

[2] Recent studies have called attention to the strong relationship between Arctic ozone loss and the volume of air experiencing temperatures below the threshold for polar stratospheric cloud formation (V-PSC) in a given winter [*Rex et al.*, 2004]. In particular, the winter of 2004–2005 saw unprecedented levels of both V-PSC and Arctic ozone loss [*Rex et al.*, 2006], underscoring concerns that future episodic reductions in Arctic column ozone may become more severe before curtailment of anthropogenic halogen production mitigates the potential for further ozone losses [*Knudsen et al.*, 2004]. At the same time, recent winters have also been characterized by a series of major warmings, with the winter of 2003–2004 showing the smallest extent of PSC temperatures for several decades [*Manney et al.*, 2005]. In order to understand these developments and monitor the potential for future ozone loss, it is essential to document as completely and accurately as possible the evolution of Arctic vortices and the PSC-conducive temperatures that accompany them [*Rex et al.*, 2002].

[3] Temperature data for computation of V-PSC are typically taken from meteorological analyses such as that provided by the European Centre for Medium-Range Weather Forecasts (ECMWF). In polar regions, however, a lower amount of assimilated data increases the uncertainty of such analyses. In particular, radiosonde, pilot balloons, and profiler data do not cover the Arctic Ocean, and aircraft reports rarely reach latitudes north of 70°N during the polar night; furthermore, infrared and microwave radiances from polar-orbiting satellites are more difficult to interpret over snow and sea ice [*Anthes et al.*, 2008]. As a consequence, validation of global analyses is difficult in many areas of the Arctic, and the impact of these errors on our scientific understanding of polar processes remains a subject of active research [*Knudsen et al.*, 2004; *Manney et al.*, 2005].

[4] Here we examine the potential of temperature data from GPS Radio Occultation (GPSRO) retrievals to enhance estimates of V-PSC in the Arctic (north of 65°N). GPSRO are active limb soundings in which a GPS receiver aboard a

[1] Jet Propulsion Laboratory, California Institute of Technology, Pasadena, California, USA.
[2] Institut für Physik der Atmosphäre, DLR, Oberpfaffenhofen, Germany.
[3] National Research Council, National Academy of Sciences, Washington, D. C., USA.
[4] Arctic Research Centre, FMI, Sodankylä, Finland.

0148-0227/09/2008JD011261$09.00

low Earth orbit (LEO) satellite tracks the GPS radio signals as they occult behind the Earth's atmosphere. The atmospheric density gradients delay and bend the radio signal; the bending angle can be inferred from the Doppler-shifted signal delay [e.g., *Fjeldbo and Eshleman*, 1965; *Kursinski et al.*, 2000], and converted into radio refractivity, N, as a function of height. Refractivity profiles can then be used to infer high vertical resolution temperature profiles from the midtroposphere to the stratosphere along 200- to 300-km-long ray paths. While radiosondes in the Arctic are subject to frequent bursts at heights between 21 and 25 km [e.g., *Randel and Wu*, 1999], GPSRO typically reach above these heights. They also seem ideally suited for polar studies because they provide dense, accurate sampling over remote regions where PSCs can form.

[5] In this study, the number of profiles and masses of air with temperatures crossing the PSC threshold are derived from GPSRO and compared to those inferred from the semidaily ECMWF-TOGA data set obtained from the DSS UCAR server (the pressure levels of the ECMWF analysis made widely available to the U.S. research community), interpolated to the location of each GPSRO profile. Validation procedures for the GPSRO profiles typically involve comparison with the analysis data itself, and we explore the implications of several validation criteria for providing value-added information to the analyses while adequately addressing quality control issues pertaining to the GPS retrievals. The ability of GPSRO to provide robust temperature profiles throughout the lower and middle Arctic stratosphere, and in particular to capture the smaller-scale temperature fluctuations which may be conducive to the formation of PSCs during active winters, are used to highlight the potential for GPSRO to facilitate the monitoring of conditions in the polar vortex that may impact future Arctic ozone losses and their possible relation to ongoing climate change processes [*Rex et al.*, 2004].

2. Background

[6] PSCs play an important role in the processes leading to ozone depletion in the polar stratosphere [*Montzka et al.*, 2003; *Rex et al.*, 2004]. Because of their role in modulating ozone concentrations, proper characterization of the thermodynamic background in which they form and evolve is necessary to better understand the ozone budget and improve prediction capabilities. We consider temperature thresholds related to three classes of PSCs: liquid supercooled ternary solutions (STS) [e.g., *Tabazadeh et al.*, 1994; *Carslaw et al.*, 1994], solid nitric acid trihydrate (NAT) [*Hanson and Mauersberger*, 1988], and ice particles. The formation mechanism of solid PSC particles has long been a matter of debate. Previous studies [*Larsen et al.*, 2004; *Drdla and Browell*, 2004], have shown that homogenous freezing mechanisms above the ice frost point temperature could explain observations of solid particles formed under synoptic-scale conditions. An alternative pathway for NAT formation is heterogeneous nucleation on ice particles. In the Arctic polar vortex widespread NAT particle formation on ice is possible under mountain wave cooling conditions [*Carslaw et al.*, 1999; *Dörnbrack et al.*, 2001]. While balloon-borne sondes, some airborne platforms, and LIDAR instruments can measure the temperature fluctuations in these waves at restricted times and Arctic locations, geographically representative estimates of V-PSC typically require comprehensive fields from global analyses such as the ECMWF. However, temperature biases in ECMWF confirmed in comparisons against observational data [*Knudsen*, 2003, and references therein] and other analyses [*Manney et al.*, 2003], along with the lower vertical resolution of its publicly available version (>1.5 km), can impact the resulting V-PSC estimates.

[7] In this work we describe the use of GPSRO during the period October 2001 to March 2005 as an additional source of data to investigate the mass, location, and morphology of air with temperatures conducive to PSC formation. GPSRO provides atmospheric temperature profiles up to the stratosphere, much like radiosondes, and with denser coverage. Temperature profiles derived from GPSRO typically agree with coincident radiosondes to within 1 K up to 24 km [e.g., *Kursinski et al.*, 1996; *Rocken et al.*, 1997]; they have also been shown to capture accurately the temperature signatures of gravity waves up to 35 km [*Preusse et al.*, 2000; *Tsuda et al.*, 2000; *de la Torre et al.*, 2004; *Namboothiri et al.*, 2008; *Hei et al.*, 2008]. The sources of error for GPSRO in general have been extensively documented [e.g., *Kursinski et al.*, 1996, 1997; *Hocke*, 1997; *Kursinski et al.*, 2000; *Hajj et al.*, 2004; *Gobiet and Kirchengast*, 2004; *Schrøder et al.*, 2007]; those pertaining to the polar stratosphere are discussed below.

[8] The retrieved GPSRO bending angles are inverted to derive atmospheric refractivity using the Abel integral transform, which requires extrapolating some values up to the top of the atmosphere [*Fjeldbo and Eshleman*, 1965; *Hajj et al.*, 2002; *Schrøder et al.*, 2007]. Above 25 km, however, the measured occultation bending angles can display high-frequency variability that increases with height. This variability can be caused by both ionospheric activity and by natural stratospheric fluctuations, and can produce biases in the stratospheric GPSRO temperature profiles [*Kursinski et al.*, 1997; *Hocke*, 1997]. Careful treatment of the Abel bending angle integral in this region is needed to minimize errors in the retrieved stratospheric refractivity. One approach uses a statistical optimization technique [*Gobiet and Kirchengast*, 2004, and references therein] to create an average between a climatological model and the GPSRO data, weighted to minimize RMS differences between retrieved bending angles and the model. The averaging gives large weights to the model at altitudes and seasons with high fluctuations and slowly transitions to occultation data at lower altitudes, depending on the RMS values for the retrieved bending angles from each occultation.

[9] An alternative approach to the Abel transform [*Hajj et al.*, 2002] extrapolates the bending angle upward from a height range where the GPSRO retrievals are known to have typically low RMS, using exponential decay with a constant scale height. This approach is less likely to filter out the natural stratospheric fluctuations which affect refractivity; it has been validated to provide the lowest model independent temperature biases when the fit is made near the stratopause (44–55 km) [*Schrøder et al.*, 2007], and shows a smaller temperature bias than the statistical approach in numerical simulations [*Ao et al.*, 2006]. We used the extrapolation approach to generate GPSRO refractivity profiles with <1 km vertical resolution from the data captured by GPS receivers

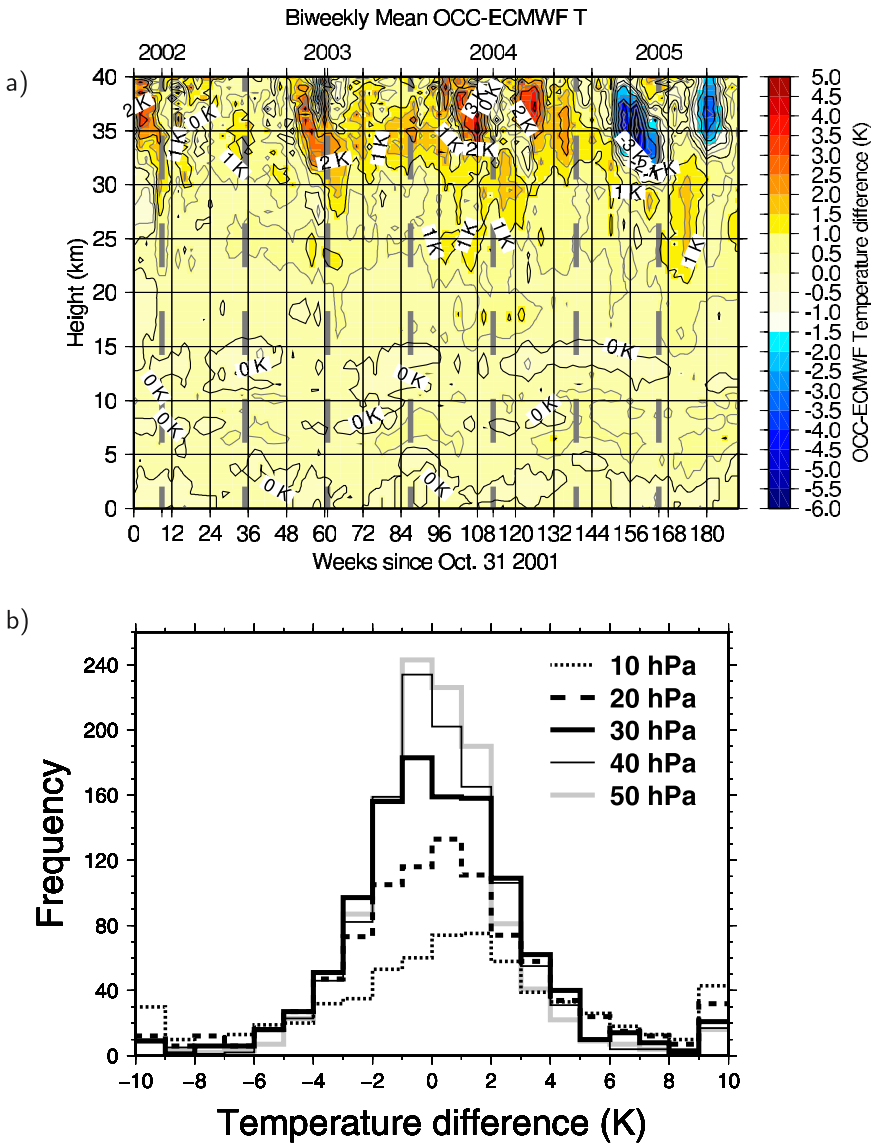

Figure 1. (a) Biweekly averaged GPSRO temperature minus ECMWF interpolated to the location and heights of the GPSRO profiles over the whole region north of 65°N. Thin contours around each color are each half degree, thick contours are each degree and their temperature difference is annotated. (b) Histogram of differences, radiosondes minus coincident GPSRO without quality control criteria. Differences larger than 10 K were counted as 10 K. Radiosondes were extrapolated to the GPSRO location using ERA-40 temperature gradients at each height.

aboard the LEO satellites CHAMP (Challenging Mini-Satellite Payload for Geophysical Research and Application) and SAC-C (Satélite de Applicaciones Científicas-C). The extrapolation was initialized at 55 km with a decay constant determined from a fit to bending angles measured at 10 height levels; the resulting parameters differed only slightly from those used by *Hajj et al.* [2004], who found that differences between coincident GPSRO retrievals from the two receivers used in this study had a standard deviation of less than 0.2 K.

[10] The derived radio refractivity, N, depends on total pressure p, water vapor pressure, e, and temperature T, as

$$N = a_1 \frac{p}{T} + \left(a_2 + \frac{a_3}{T}\right)\frac{e}{T}, \qquad (1)$$

with a_1 = 77.6 K/hPa, a_2 = −12.81 K/hPa, and a_3 = 3.739 x10^5 K^2/hPa [*Thayer*, 1974; *Bevis et al.*, 1994]. In the stratosphere, the water vapor contribution is too small to be detected and can be ignored, so that the refractivity N is proportional to atmospheric density. The conversion from density to temperature, however, requires performing the hydrostatic balance integral [*Fjeldbo and Eshleman*, 1965; *Hajj et al.*, 2002]. To initialize this integral the temperature from the occultation is assumed equal to that of the ECMWF-TOGA interpolated to the location of the occultation at the initialization height, z_o = 41 km for our specific data set. The error due to this assumption can be shown to decay inversely with the density, so that its impact is typically found to peak

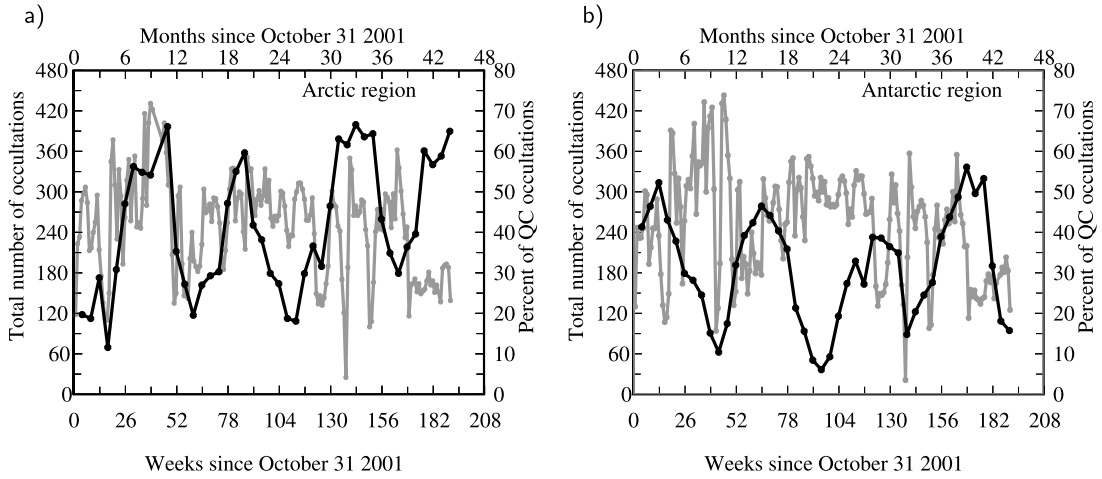

Figure 2. Total number of weekly occultations (a) north and (b) south of 65°S (in grey), and percentage of occultations (monthly averaged) within 10 K and 10% refractivity agreement with the model at all heights between 41 km and 4 km (in black).

within the first scale height below the initialization height (see Figure 1a).

3. Validation

[11] Differences between the ECMWF analysis and GPSRO-derived temperatures during the period of our study, averaged over the region poleward of 65°N, are shown in Figure 1a. For this comparison the ECMWF data closest in time to each occultation were interpolated to the location and height of the retrieved profile and subtracted, with the differences averaged on a biweekly basis into 0.5-km-altitude bins. The comparison was limited to occultations which differed from the interpolated ECMWF analysis by less than 10 K and 10% refractivity calculated from equation (1) at all heights above 4 km. Mean differences with the validated data are sub-Kelvin at most heights below 30 km, with the analysis typically being colder than the occultations. This cold bias of ECMWF against GPSRO agrees with results for shorter time periods in comparisons against CHAMP GPSRO [*Gobiet et al.*, 2005] and against radiosondes [*Knudsen*, 2003]. The largest differences are found typically near 35 km, where a seasonal behavior is observed: each winter's occultations seem to be consistently warmer or colder than the analysis, suggesting that the model may not fully capture the amplitude behavior of seasonal temperature variability in the midstratosphere.

[12] As an independent validation, comparisons of GPSRO with radiosonde-derived temperatures in the stratosphere are shown in Figure 1b for the region poleward of 65°N, during the period April 2001 to August 2002 when GPSRO and ERA-40, the ECMWF reanalysis, overlap; no screening of the GPSRO retrievals was performed, but differences larger than 10 K were counted as 10 K. Given the paucity of radiosonde data, for this comparison "coincident" radiosonde soundings were considered if they occurred within 500 km and 6 hours of a GPSRO retrieval, with the sonde data then being extrapolated horizontally to the location of the GPSRO profile using temperature gradients from ERA-40. Note the larger spread in the upper stratospheric values, consistent with a smaller signal-to-noise ratio for GPSRO at these altitudes [*Hajj et al.*, 2002]. Few occultations are seen with temperature differences larger than 4 K (9% at 50 hPa, 11% at 40 hPa, 14% at 30 hPa, 22% at 20 hPa and 36% at 10 hPa) showing that most GPSRO substantially agree with nearby radiosonde retrievals.

[13] The impact of ECMWF stratospheric temperature biases on the estimates of air mass conducive to PSCs has been previously documented for this timeframe using comparisons to radiosondes [*Knudsen*, 2003, and references therein]. Especially for the Arctic, GPSRO provides a more comprehensive spatial coverage than the radiosonde network, with higher vertical resolution capable of capturing fluctuations which may be responsible for the formation of subgrid-scale PSCs not documented by the global analyses. The lack of independent observational data, on the other hand, restricts our ability to validate the GPSRO, leading to a situation in which the analysis data itself must be used to screen the GPSRO retrievals for outliers. A particular drawback of this approach is the risk of discarding GPSRO profiles that capture errors in the analysis. Figure 2 illustrates this by showing a consequence of the seasonal behavior described in Figure 1a. The black line shows the percentage of GPSRO profiles where temperatures and refractivities were within 10 K and 10% respectively, of the interpolated analysis at all heights between 4 km and 41 km, for the Arctic (Figure 2a) and the Antarctic (Figure 2b), compared with the number of weekly occultations in grey. The total number of retrieved profiles follows a variability which can be traced back to operational changes; on the other hand, the percentage of profiles meeting the 10K-10% criterion is systematically lower in the winter months of both hemispheres, following a cycle independent of the operational changes. There is no reason why occultations should underperform in local polar winter conditions; given the good agreement between GPSRO and radiosondes shown in Figure 1b, we believe that the discrepancies found

Table 1. Number of Occultations Passing Different Selection Criteria in December 2001[a]

Upper Limits	Criterion 1	Criterion 2	Criterion 3
41 km and $\lvert\varepsilon_N\rvert \leq 3$	220	159	156
41 km and $\lvert\varepsilon_N\rvert \leq 5$	220	207	203
32 km and $\lvert\varepsilon_N\rvert \leq 3$	759	325	202
32 km and $\lvert\varepsilon_N\rvert \leq 5$	759	491	280

[a]The number reflects how many of the initial 1200 passed each subsequent selection criterion (when applied from left to right).

are more likely to reflect errors in the weather analysis temperatures than in the GPSRO.

4. Data Selection Criteria

[14] Even with a statistically better agreement between radiosondes and GPSRO, occultations are subject to possible errors arising at various stages of the GPSRO data reduction process [e.g., *Kursinski et al.*, 2000; *Hajj et al.*, 2002]. The error sources of GPSRO soundings can be caused mainly by instrumental malfunction (such as loss of tracking and phase slips) or by retrieval uncertainties (such as occasional large ionospheric scintillations or the model induced errors via the initialization of the hydrostatic integral). A typical screening of the data to reduce the impact of such errors is made by assuming that large differences between an operational weather analysis and the GPSRO profiles may indicate individual outliers. *Hajj et al.* [2004] describe an operational screening approach to remove possible faulty GPSRO retrievals by comparing against weather analysis data. In order to balance the requirements for quality control of the GPSRO profiles with the need to maximize the benefit provided by the observational data that capture conditions missed by the weather analyses, we examined the consequences of a number of validation criteria for the retrievals.

[15] The first criterion (from now on termed criterion 1) required GPSRO and the interpolated ECMWF-TOGA to be within 10 K in temperature and within 10% in refractivity of each other over a height range extending either from 11 km to 41 km in one case or from the higher of 11 km and the lapse rate tropopause to 32 km in the relaxed case. This range of heights is chosen to be sure that it covers over the whole vertical extent where the coldest temperatures are found. Criterion 2 required additionally that refractivity differences at 41 km (the temperature initialization height) be under a given threshold absolute value ε_N (either 3% or 5%). For criterion 3, the mean absolute deviation from ECMWF-TOGA over the 37- to 41-km range was additionally required to be less than 5 K for each profile, thus eliminating the GPSRO soundings with large sharp temperature structures within their uppermost few kilometers. These criteria, which skew the comparison toward ECMWF-like profiles, ensure that the differences are mostly due to features substantially smaller than the scale height where anomalies often exceed 1 K and can be important contributors to PSC formation [e.g., *Carslaw et al.*, 1999; *Dörnbrack et al.*, 1999, 2001].

[16] Table 1 shows the number of GPSRO measurements available for the month of December 2001, based on the successive application of the three criteria. For illustration, out of 1200 profiles captured north of 65°N, only 220 passed the first criterion with upper boundary at 41 km, while 207 (159) passed the first two using threshold values of 5% (3%), and of these 203 (156) passed the third criterion as well. Inspection of the GPSRO profiles that failed these criteria showed that many had large amplitude temperature fluctuations in the height range from 32 km (approximately the 10-hPa level) up to 41 km. When the test for criterion 1 is applied up to a height of only 32 km, therefore, the number of passing profiles increased dramatically to 759; however since criteria 2 and 3 are still applied in the upper stratosphere (at or near 41 km), the total number of profiles passing all three tests increased only slightly.

[17] As an example of the benefits to be gained by using analysis data to screen the GPSRO retrievals, Table 2 shows mean and median statistics for $\mathcal{N}$ differences of the extrapolated radiosonde soundings used in Figure 1b with both ECMWF and GPSRO temperatures without filtering based on the differences to ECMWF, while Table 3 shows the statistical moments for cases where the difference fulfilled the "relaxed" version of criterion 1. Interestingly, the GPSRO are closer in the filtered and unfiltered versions to the radiosondes above 40 hPa in both mean and median than the analysis, in spite of the fact that the analysis assimilates the radiosonde data at these heights. Standard and absolute deviations are larger for the GPSRO data, in part because GPSRO captures temperature fluctuations (e.g., gravity waves) that the model parameterizes, thus eliminating sources of horizontal variability. The filtered retrievals in Table 3 are generally closer to the radiosondes than the unfiltered with the standard deviation of the GPSRO-radiosonde differences, in particular, being strongly reduced by the removal of outliers associated with faulty profiles. These results demonstrate that judicious use of screening by model data can enhance the ability of the GPSRO retrievals to provide value-added data to the analysis itself.

[18] The geographical distribution of the profiles passing the various criteria is shown in Figure 3 for December 2001. The black symbols in each panel show profiles which passed criterion 1 only, while color symbols indicate profiles which satisfied all three criteria, using the parameters listed in the corresponding row of Table 1. The densest geographical coverage (759 profiles) results from applying only the relaxed version of criterion 1, with height range from the higher of 11 km or the lapse-rate tropopause to 32 km (all symbols in Figures 3c and 3d). Given that Figures 1a and 2 and Table 2 suggests that GPSRO agrees better with nearby radiosondes than the analysis in the middle to upper stratosphere during polar winter, disqualifying GPSRO profiles on the basis of the most restrictive quality control

Table 2. Statistical Moments of the Differences From Radiosondes to GPSRO and Analysis for the Same Timeframe and Conditions as in Figure 1b

	Radiosonde-GPSRO and Radiosonde-ECMWF (K)				
hPa	Mean	SD	Median	Mean Absolute Deviation	$\mathcal{N}$
10	0.76 1.21	7.99 2.21	0.84 1.13	4.48 1.89	667
20	0.49 0.63	8.84 1.95	0.38 0.53	3.18 1.68	920
30	−0.05 0.60	18.59 1.73	0.09 0.54	2.54 1.54	1135
40	0.32 0.22	5.10 1.64	0.05 0.14	2.14 1.44	1175
50	0.31 0.14	4.78 1.74	0.01 0.12	1.96 1.41	1184

Table 3. Statistical Moments of the Differences From Radiosondes to GPSRO and Analysis for the Same Timeframe and Conditions as in Figure 1b When the Analysis and Occultation are Within 10 K and 10% Refractivity Differences at All Heights Between 11 km and 32 km

	Radiosonde-GPSRO and Radiosonde-ECMWF (K)				
hPa	Mean	SD	Median	Mean Absolute Deviation	$\mathcal{N}$
10	0.52 1.11	3.96 2.24	0.75 1.08	3.85 1.81	371
20	0.08 0.50	2.87 1.93	0.17 0.42	2.52 1.60	535
30	0.00 0.49	2.43 1.75	0.05 0.44	2.34 1.57	674
40	−0.05 0.12	2.05 1.63	−0.06 0.08	1.95 1.47	699
50	−0.1 0.01	2.19 1.82	0.00 0.01	1.73 1.39	705

criteria might miss some important geophysical information. Recall, however, that the error bar of individual profiles of GPSRO stratospheric temperatures increases for such occultations as a result of the possible role of the ionosphere in causing bending angle fluctuations, and the effect of temperature initialization through the analysis which is most likely to introduce biases close to the initialization level (41 km).

[19] Figure 4 shows maps with the locations where PSC temperatures were found in December 2001 using the upper (41 km, Figure 4a) and lower (32 km, Figure 4b) cutoff heights for Criterion 1 only. We calculated the temperature thresholds as a function of height for nitric acid trihydrate PSCs (NAT or type I, $T < T_{NAT}$) derived from GPSRO and the interpolated ECMWF-TOGA profiles. NAT PSC formation depends on pressure and chemical composition of the air. Because GPSRO does not measure atmospheric composition, and there are no coincident measurements of the chemical species along the occultation profile, one cannot claim PSC formation, and we focus on temperature thresholds. In Figure 4, we used the Hanson-Mauersberger critical temperature for PSC formation [*Hanson and Mauersberger*, 1988], assuming typical stratospheric concentrations of 10 ppbv HNO_3 and a constant H_2O concentration of 5 ppmv

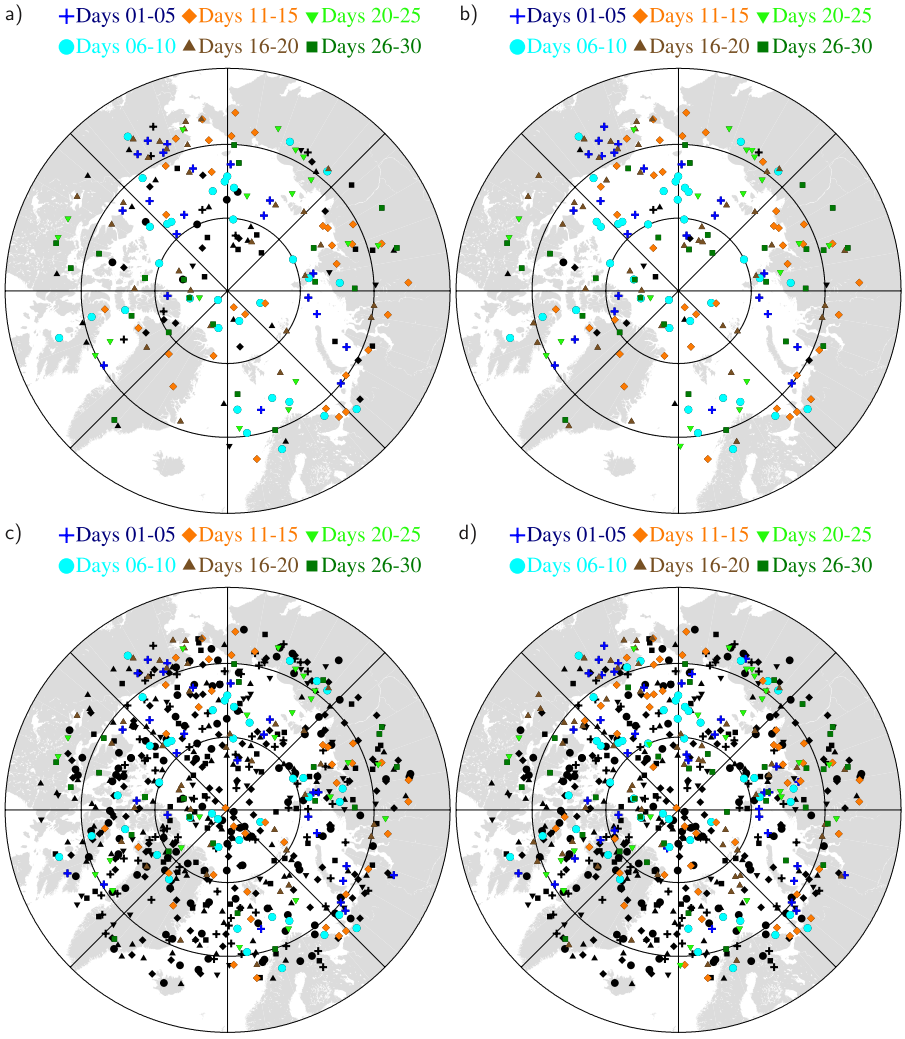

Figure 3. Locations of the occultations studied for December 2001. Different symbols for each 5-day group. Black shows the locations where only criterion 1 (temperature differences less than 10 K and refractivity differences below 10%) is required, and color shows the profiles remaining after all criteria 1–3 of Table 1 are applied. Limits are (a) 41 km ($|\varepsilon_N| \leq 3$), (b) 41 km ($|\varepsilon_N| \leq 5$), (c) 32 km ($|\varepsilon_N| \leq 3$), and (d) 32 km ($|\varepsilon_N| \leq 5$).

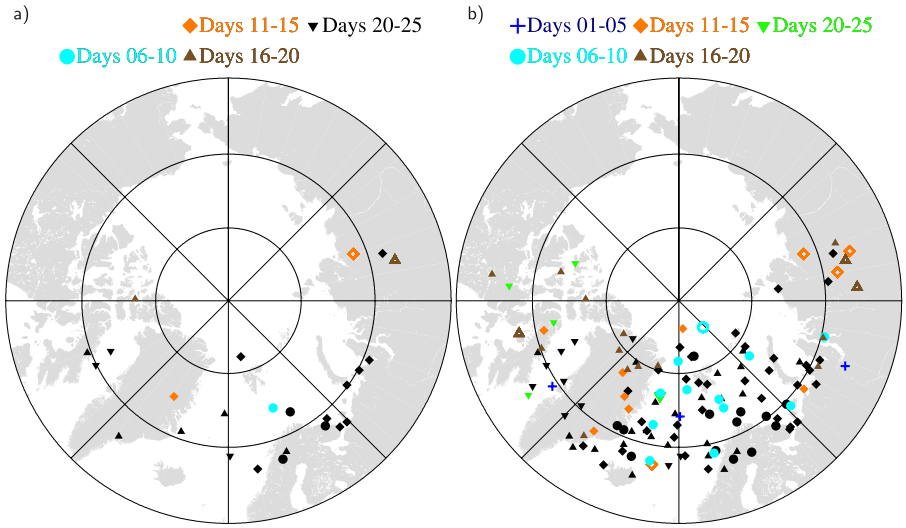

Figure 4. Latitudes and longitudes where the Hanson-Mauersberger criterion was met by GPSRO (color) in December 2001. Color legends at top distinguish days with some profiles where only one of the two data sets found temperatures conducive to PSCs. Large open symbols denote that the criterion was met only by ECMWF. Black symbols mark locations where both the interpolated ECMWF-TOGA and GPSRO met the criterion. (a) Using selection criterion 1 only for the limits in first row of Table 1 (i.e., differences below 10 K in temperature 10% in N between 11 km and 41 km). (b) Using the same selection criterion for the limits in fourth row of Table 1 (i.e., differences below 10 K in temperature 10% in N between 11 km and 32 km).

[e.g., *Voigt et al.*, 2000; *Müller et al.*, 2001]. We also tested for ice PSC temperatures (type II PSCs, $T < T_{ICE}$, the ice saturation temperature at 5 ppmv H_2O). Such temperatures were found near the lapse rate tropopause height (i.e., they are likely associated with cirrus) or in occultations with too large temperature fluctuations to pass our selection criteria; hence they were not considered further.

[20] For both cutoff heights applied to criterion 1, the PSC-conducive profiles were found predominantly between 90°W and 120°E, occurring preferentially above the North Atlantic and above land masses identified in a separate study as major centers of gravity wave activity [*Wu and Zhang*, 2004]. While the majority of the PSC-conducive profiles were identified in both the analysis and occultation data (black symbols), a significant number (solid color symbols) were identified by GPSRO only, with fewer (open color symbols) rejected by GPSRO but having PSC-prone temperatures in the analysis: in particular, the fraction of occultations detecting PSC temperatures not found in the model increased from 12% to 31% as the validation height was reduced from 41 km to 32 km; showing the greater impact of GPSRO on the analysis when using the relaxed version of this criterion. Many of the PSC profiles found only by GPSRO occur near PSC profiles identified by both techniques in Figure 4b, indicating that most GPSRO profiles with temperatures conducive to PSCs are plausible even under the most relaxed selection criterion. Note that the different 5-day groupings of PSC profiles tend to occur in proximity with each other, indicating that they may be associated with transient wave activity or other localized sources of perturbation.

[21] To examine the impact of using different thermodynamic criteria for PSC formation, we show in Figure 5 the daily number of profiles in December 2001 which crossed the temperature threshold for NAT PSCs (Figure 5, top), and the number crossing the STS threshold, defined as $T_{STS} = T_{NAT} - 3.5$ K [*Tabazadeh et al.*, 1994; *Carslaw et al.*, 1994], in Figure 5 (bottom); profiles validated using criterion 1 up to 41 (32) km are shown in the left (right) column of Figure 5, with grey bars denoting validated GPSRO retrievals and black bars the corresponding interpolated ECMWF profiles. The greatest (proportionate) differences are seen for the more restrictive PSC (STS) and the less restrictive GPSRO (11–32 km) criteria (Figure 5d), in which the majority of PSC profiles detected by GPSRO are not found by the analysis. Several additional factors that can influence these thresholds (e.g., variations in HNO_3 and H_2O concentration with distance from the polar vortex [*Lahoz et al.*, 1994], and wind speed variations with latitude that can influence the total air mass exposed to PSC-forming temperatures) will be considered in future studies.

[22] Figure 6 shows the effect of adding successively criterion 2 (Figure 6a) and criterion 3 (Figure 6b) to the validating procedure for the profiles shown in Figure 5, using the 32-km cutoff height for criterion 1. Again, the more restrictive PSC criterion and the less restrictive GPSRO criteria produce the greatest differences between the two data types, with GPSRO consistently showing more profiles prone to PSC formation than found by ECMWF-TOGA. In particular, most of the STS PSC conditions found by GPSRO during the second half of December 2001 are absent in the analysis, suggesting that they are associated with waves. The relatively low number of vertical levels included in the ECMWF-TOGA is one possible cause for this discrepancy; however, since the full ECMWF analysis uses parameterized representations of gravity waves, it is unlikely to capture the specific fluctuations measured by the observations. Another cause might be that the coarse horizontal resolution in the

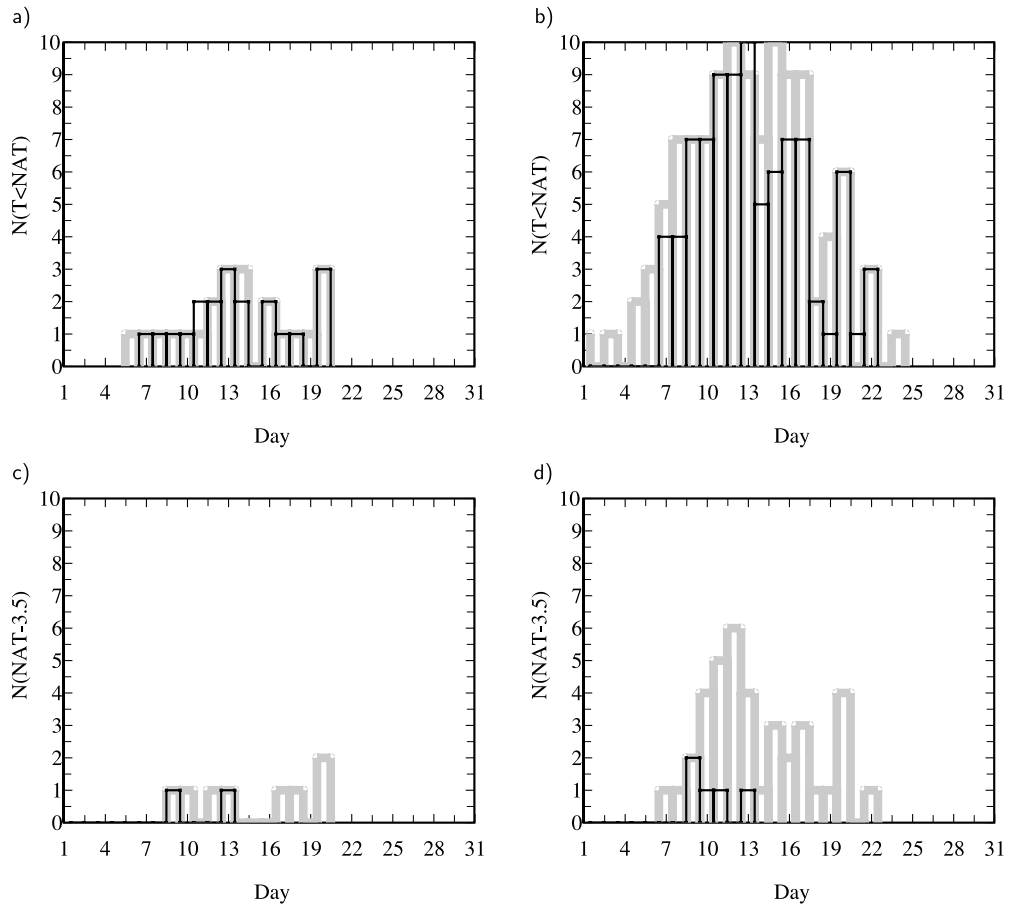

Figure 5. Number of daily profiles with temperatures conducive to PSC formation in December 2001 under criterion 1. Grey denotes GPSRO; black denotes the interpolated ECMWF-TOGA. (a, c) For the limits in first row of Table 1 (i.e., differences below 10 K in temperature 10% in N between 11 km and 41 km); (b, d) for the limits in fourth row of Table 1 (i.e., differences below 10 K in temperature 10% in N between 11 km and 32 km). Figures 5a and 5b are under the Hanson-Mauersberger threshold for NAT PSCs at 5 ppmv water vapor and 10 ppbv HNO_3; Figures 5c and 5d are under the STS threshold ($T_{NAT} - 3.5$ K).

original ECMWF analysis inhibits dynamical processes that produce small-scale structures such as mountain waves, whose simulated spectrum strongly depends on the horizontal resolution of the model runs. Finally, we note that similar comparisons with NCEP (not shown) displayed even larger differences with the GPSRO retrievals.

5. Impact of GPSRO on Detection of PSC Temperatures

[23] Figures 5 and 6 show the impact of different criteria on PSC-temperature detection by GPSRO and the ECMWF analysis during December 2001, a month which saw relatively disturbed conditions and only a warm weak vortex developing [*Naujokat et al.*, 2002]. To investigate the differences between the occultation and model data under different regimes, we plot the percentage of validated GPS profiles which detected PSC temperatures for the winter months during each year of our study using relaxed criterion 1 and STS temperature thresholds (red solid lines), along with the corresponding results for the interpolated model profiles (black solid lines), in Figure 7. Corresponding values for the mass of air crossing the STS threshold, summed over the same profiles for each month, are shown by the dashed lines. The different vertical scaling used for each winter shows an intriguing pattern of alternating high and low percentages and masses of air with STS temperatures for the successive years shown in the individual panels. This apparent 2-year cycle is consistent with the known influence of the Quasi-Biennial Oscillation (QBO) on the temperature of the polar Arctic stratosphere, which maximizes in late fall/early winter [*Garfinkel and Hartmann*, 2007]. The QBO was in its east phase during the winters of 2001/2002 and 2003/2004, while it was in its west phase in 2002/2003 and 2004/2005 [*Labitzke*, 2005].

[24] During the warm winters (Figures 7a and 7c) the percentage of PSC profiles (i.e., with temperatures falling below the STS threshold) detected by GPS was considerably larger than that found from the coincident model data, with both maximizing in December of their respective years. During the cooler winters (Figures 7b and 7d) the percentage of STS profiles is roughly an order of magnitude greater, with maxima falling in December 2002 and January 2005.

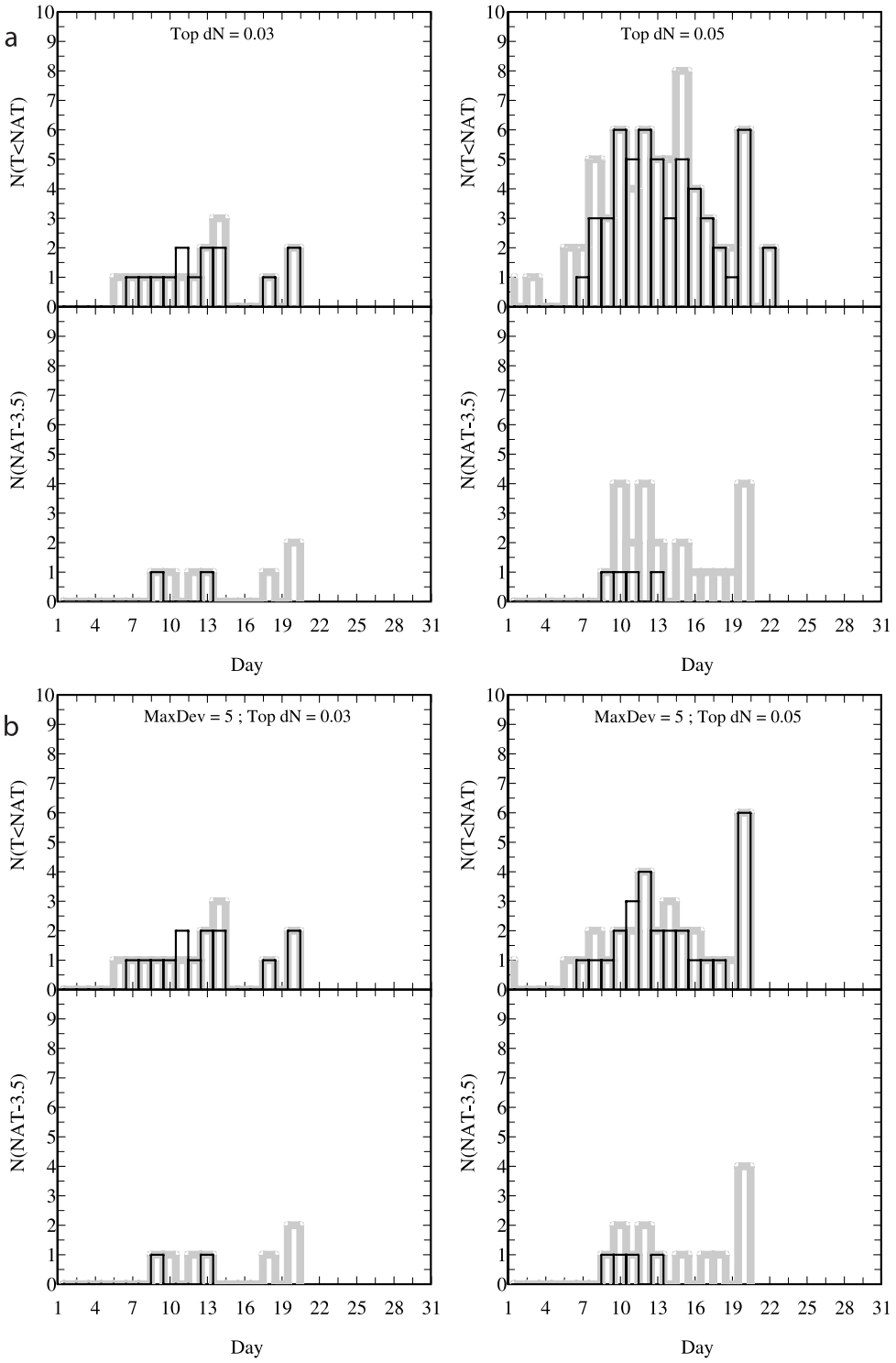

Figure 6. Same as in Figure 5 but adding selection criteria 2 and 3 from third and fourth rows of Table 1. Grey is GPSRO; black is the interpolated ECMWF-TOGA. (left) For third row of Table 1; (right) for fourth row of Table 1. (a) Hanson-Mauersberger and STS thresholds for PSCs when selection criterion 2 is added to the criterion 1 in Figure 5. (b) The same as Figure 6a when selection criterion 3 is added to criteria 1 and 2.

For these winters the GPS tends to detect fewer profiles with STS temperatures, although the proportional differences between the observed and modeled profiles are smaller. The change of sign in the biases between GPSRO and ECMWF during the cold winters is consistent with the general cold bias relative to GPSRO noted for the model in Figure 1a. Cold model biases at the poles have been reported before and connected to an underrepresented gravity wave drag which

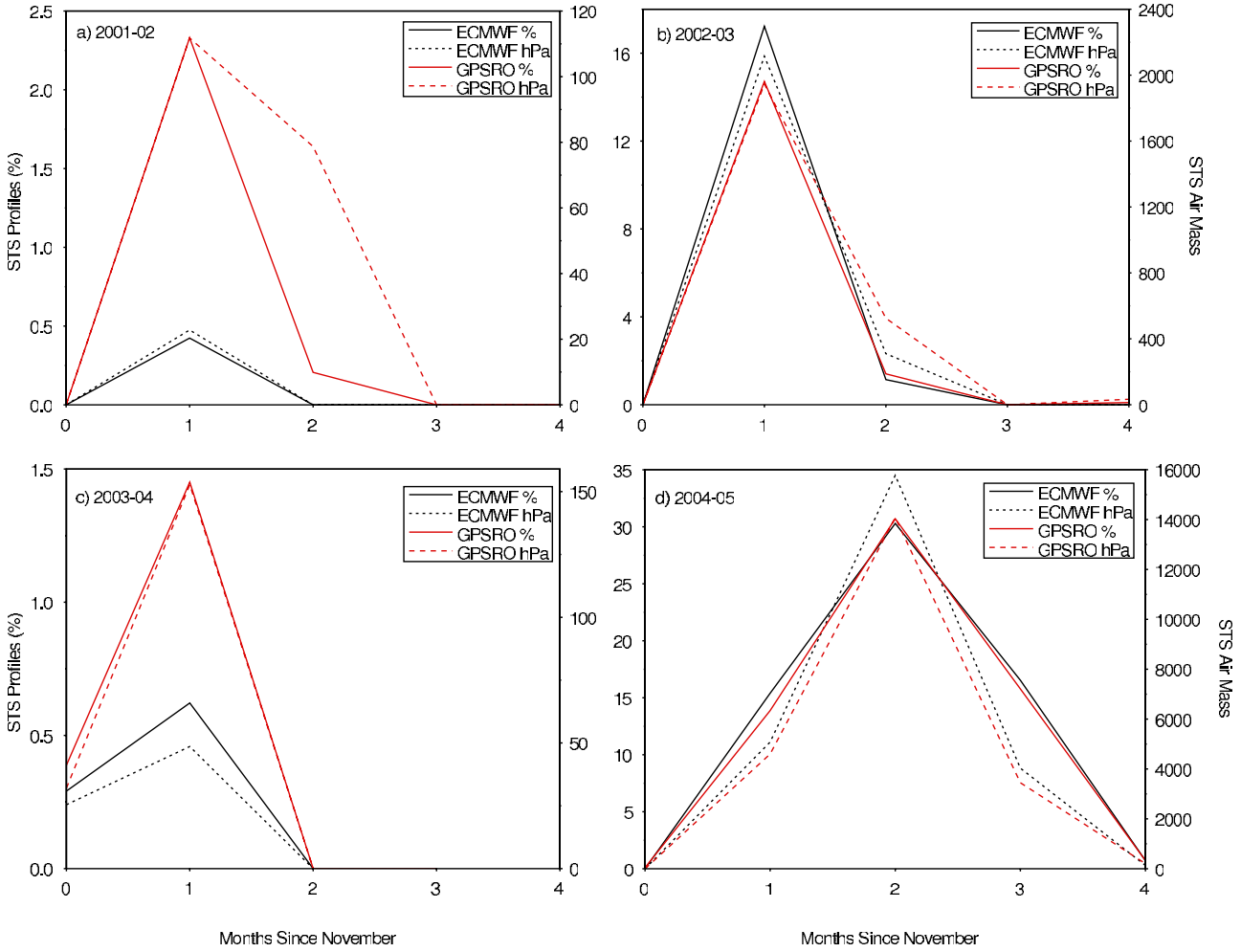

Figure 7. Monthly percentage of profiles (solid lines, left axes) and sum of air masses (dashed lines, right axes) which had PSC temperatures ($T < T_{STS}$) during the Arctic winter months between November 2001 and March 2005. GPSRO profiles (red lines) were screened using relaxed version of criterion 1 (see text), and ECMWF profiles were interpolated to the time and location of the validated GPSRO data. For these curves a constant water vapor mixing ratio has been assumed.

would lead to a stronger polar jet and thus a cold bias in polar stratospheric temperatures [*García and Boville*, 1994].

[25] Figure 8 shows that the percentage differences maximize in December and have roughly similar absolute magnitudes for all winters, with the GPS finding more STS profiles during warm winters and fewer during the cold winters. Similar results are found when the total mass of PSC-prone air detected during each month from the two data sources is considered, although the mass of STS-cooled air during the strong-vortex winter of 2005, shown in Figure 7d (right axis), is about 2 orders of magnitude larger than that found for the weaker-vortex cases.

[26] Further insight into the dynamical behavior that gives rise to enhanced detection of PSC-prone air by GPSRO may be gained by examining the time dependence of Arctic stratospheric temperatures during the disturbed winters of 2001/2002 and 2003/2004. Figure 9 shows the dramatic changes in stratospheric temperatures which occurred in December of both winters. For instance, an increase of 35 K is evident at 30 km altitude across the entire Arctic at the end of December 2001, showing the effects of an unusually strong early warming during that winter [*Naujokat et al.*, 2002]. The similar large temperature increases visible in December 2003 show the effects of one of the strongest midwinter warmings in recent decades [*Manney et al.*, 2005].

6. Discussion and Conclusions

[27] Our results show that for warm winter conditions (typically associated with weaker/disturbed-polar vortex), as prevailed in December 2001 to March 2002 and again in December 2003 to March 2004, GPS RO detects more STS-conducive air than is seen in the corresponding profiles from the ECMWF analysis. On the other hand, for cold winter (strong vortex) cases, such as occurred in December 2002 to March 2003 and again in December 2004 to March 2005, the model captures the full extent of PSC-prone air as found from the GPS RO data. These results indicate that while the model is fully capable of capturing the large-scale temperature anomalies that accompany strong Arctic polar stratospheric vortices, it does not resolve the PSC-prone

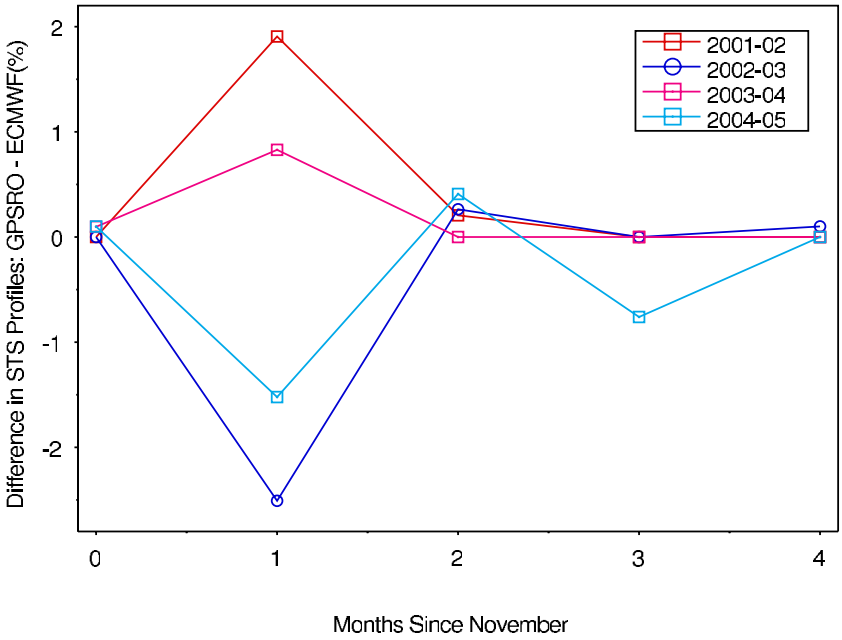

Figure 8. Differences in the monthly percentages of profiles (over the total number of soundings) with air at T < T_{STS} for the Arctic winter months between November 2001 and March 2005 under the same conditions as Figure 7.

temperatures which still occur, even in the absence of a well-formed vortex.

[28] Some insight into the relative PSC atmospheric temperature detection capabilities of the ECMWF analysis and GPSRO can be gained by examining profiles captured during the warm (disturbed vortex) winter of 2001–2002. Figure 10 shows SAC-C GPSRO and ECMWF profiles on 11 December (thick solid lines) and for the nearest occultation on 12 December (dashed lines, separated by about 500 km). Interestingly, the analysis (gray lines) approximates a running vertical mean of the GPSRO profiles (black lines) which captured features sharper and colder than available from the ECMWF-TOGA model data. These features can be interpreted as a large-scale planetary wave sampled at nearby time and space coordinates, or as two different, localized (in time and space) gravity waves arising in the disturbed conditions prevalent during that winter [*Naujokat et al.*, 2002]. Figure 10 clearly shows that the GPSRO profiles detect more pronounced and extensive PSC temperatures using the NAT criterion (right-most light solid line), and also cross the ice PSC threshold (left-most light solid line), whereas the analysis data only marginally detect NAT temperatures.

[29] These examples demonstrate that the fine-scale vertical structure of polar stratospheric temperatures impacts estimates of PSC budgets and that GPSRO can provide unique insight into what dynamical processes might be leading to PSC temperatures. The two profiles in Figure 10 passed the more relaxed criterion 1 but did not pass criteria 2 and 3 because the analysis does not solve for gravity waves. Thus, by applying quality control procedures based on the analysis data which do not reject profiles with high

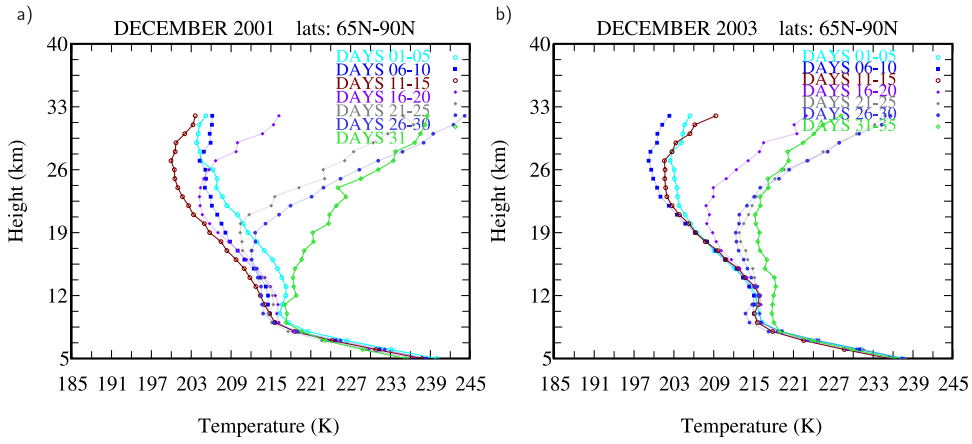

Figure 9. Five-day averaged GPSRO temperature profiles showing the major warmings for December (a) 2001 and (b) 2003 over the whole region north of 65°N.

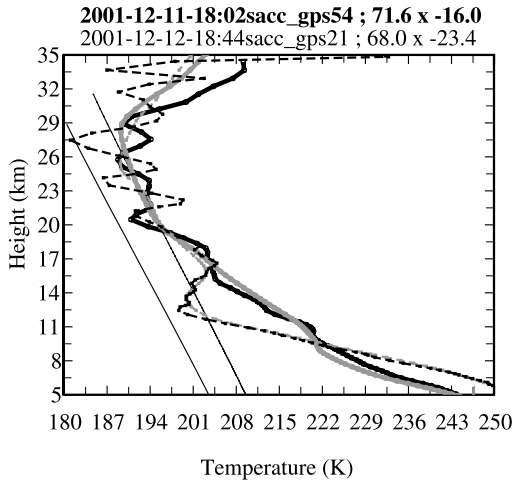

Figure 10. Occultation temperature profile (thick solid black line) with sharp temperature fluctuations that crossed below T_{NAT} and T_{ice} (thin solid black lines) at 1802 UTC 11 December 2001 at 71.6°N, 16°W. Nearby occultation 1 day later in thin dashed line at 68°N, 23.4°W. The interpolated ECMWF-TOGA is shown for both days in thick solid grey for 11 December and thin dashed grey line for 12 December. Thin black lines show the thresholds for NAT PSCs T_{NAT} in an atmosphere with 5 ppmv H_20 and 10 ppbv HNO_3, and the colder T_{ice} for ice PSCs.

variability in the midstratosphere, we are able to find fine-scale features in our retrievals that may impact PSC formation budgets while still minimizing the number of faulty GPSRO profiles. Our results show that the higher vertical resolution provided by the GPSRO technique enables more robust detection of PSC temperatures associated with the vigorous planetary and/or gravity wave activity that characterized two of the four winters under study in this case. Since assimilation of GPSRO data by ECMWF [*Healy et al.*, 2007] and other data centers such as NCEP [*Cucurull et al.*, 2008] has become operational in recent years, this enhanced capability may be expected to produce a more accurate representation of these short vertical-wavelength structures and their relation to climate-driven changes in the potential for PSC formation and ozone loss.

[30] **Acknowledgments.** We acknowledge NCAR's Data Support Section and the ECMWF for the ECMWF data. NOAA-CIRES Climate Diagnostics Center, Boulder, Colorado, USA, are from their Web site at http://www.cdc.noaa.gov/. Funding for this work has been provided by NASA through a grant and the JPL R&TD program. T.M.S. acknowledges financial support from the National Research Council program of the National Academy of Sciences. Conversations with S. S. Leroy and R. Salawitch are gratefully acknowledged. We also acknowledge the comments by the referees that helped improve this article. Part of the research described this paper was carried out at the Jet Propulsion Laboratory/California Institute of Technology, under a contract with the National Aeronautics and Space Administration.

References

Anthes, R., et al. (2008), The COSMIC/FORMOSAT-3 mission: Early results, *Bull. Am. Meteorol. Soc.*, *89*, 313–333, doi:10.1175/BAMS-89-3-313.

Ao, C. O., G. A. Hajj, B. A. Iijima, A. J. Mannucci, T. M. Schrøder, M. de la Torre Juárez, and S. S. Leroy (2006), Sensitivity of stratospheric retrievals from radio occultations on upper boundary conditions, in *Atmosphere and Climate Studies by Occultation Methods*, edited by U. Foelsche, G. Kirchengast, and A. K. Steiner, pp. 17–26, Springer, Berlin.

Bevis, M., S. Businger, S. Chiswell, T. A. Herring, R. A. Anthes, C. Rocken, and R. H. Ware (1994), GPS meteorology: Mapping zenith wet delays onto precipitable water, *J. Appl. Meteorol.*, *33*, 379–386.

Carslaw, K. S., B. P. Luo, S. L. Clegg, T. Peter, P. Brimblecombe, and P. J. Crutzen (1994), Stratospheric aerosol growth and HNO_3 gas phase depletion from coupled HNO_3 and water uptake by liquid particles, *Geophys. Res. Lett.*, *21*, 2479–2482.

Carslaw, K. S., T. Peter, J. Bacmeister, and S. D. Eckermann (1999), Widespread solid particle formation by mountain waves in the arctic stratosphere, *J. Geophys. Res.*, *104*, 1827–1836.

Cucurull, L., J. C. Derber, R. Treadon, and R. J. Purser (2008), Preliminary impact studies using global positioning system radio occultation profiles at NCEP, *Mon. Weather Rev.*, *136*, 1865–1877, doi:10.1175/2007MWR2260.1.

de la Torre, A., T. Tsuda, G. A. Hajj, and J. Wickert (2004), A global distribution of the stratospheric gravity wave activity from GPS occultation profiles with SAC-C and CHAMP, *J. Meteorol. Soc. Jpn.*, *82*, 407–417.

Dörnbrack, A., M. Leutbecher, R. Kivi, and E. Kyrö (1999), Mountain wave induced record low stratospheric temperatures above northern scandinavia, *Tellus, Ser. A*, *51*, 951–963.

Dörnbrack, A., M. Leutbecher, J. Reichardt, A. Behrendt, K.-P. Müller, and G. Baumgarten (2001), Relevance of mountain wave cooling for the formation of polar stratospheric clouds over Scandinavia: Mesoscale dynamics and observations from January 1997, *J. Geophys. Res.*, *106*, 1569–1581.

Drdla, K., and E. V. Browell (2004), Microphysical modeling of the 1999–2000 Arctic winter: 3. Impact of homogeneous freezing on polar stratospheric clouds, *J. Geophys. Res.*, *109*, D10201, doi:10.1029/2003JD004352.

Fjeldbo, F., and V. Eshleman (1965), The bistatic radar-occultation method for the study of planetary atmospheres, *J. Geophys. Res.*, *70*, 3217–3225.

García, R., and B. A. Boville (1994), "Downward control" of the mean meridional circulation and temperature distribution of the polar winter stratosphere, *J. Atmos. Res.*, *51*, 2238–2245.

Garfinkel, C., and D. Hartmann (2007), Effects of the El Niño–Southern Oscillation and the Quasi-Biennial Oscillation on polar temperatures in the stratosphere, *J. Geophys. Res.*, *112*, D19112, doi:10.1029/2007JD008481.

Gobiet, A., and G. Kirchengast (2004), Advancements of Global Navigation Satellite System radio occultation retrieval in the upper stratosphere for optimal climate monitoring utility, *J. Geophys. Res.*, *109*, D24110, doi:10.1029/2004JD005117.

Gobiet, A., U. Foelsche, A. Steiner, M. Borsche, G. Kirchengast, and J. Wickert (2005), Climatological validation of stratospheric temperatures in ECMWF operational analyses with CHAMP radio occultation data, *Geophys. Res. Lett.*, *32*, L12806, doi:10.1029/2005GL022617.

Hajj, G. A., E. R. Kursinski, L. J. Romans, W. I. Bertiger, and S. S. Leroy (2002), A technical description of atmospheric sounding by GPS occultation, *J. Atmos. Solar Terr. Phys.*, *64*, 451–469.

Hajj, G. A., et al. (2004), CHAMP and SAC-C, atmospheric occultation results and intercomparisons, *J. Geophys. Res.*, *109*, D06109, doi:10.1029/2003JD003909.

Hanson, D., and K. Mauersberger (1988), Laboratory studies of the nitric-acid trihydrate—Implications for the South Polar stratosphere, *Geophys. Res. Lett.*, *15*, 855–858.

Healy, S. B., J. Wickert, G. Michalak, T. Schmidt, and G. Beyerle (2007), Combined forecast impact of GRACE-A and CHAMP GPS radio occultation bending angle profiles, *Atmos. Sci. Lett.*, *8*, 43–50, doi:10.1002/asl.149.

Hei, H., T. Tsuda, and T. Hirooka (2008), Characteristics of atmospheric gravity wave activity in the polar regions revealed by GPS radio occultation data with CHAMP, *J. Geophys. Res.*, *113*, D04107, doi:10.1029/2007JD008938.

Hocke, K. (1997), Inversion of GPS meteorology data, *Ann. Geophys.*, *15*, 443–450.

Knudsen, B. (2003), On the accuracy of analysed low temperatures in the stratosphere, *Atmos. Chem. Phys.*, *3*, 1759–1768.

Knudsen, B., N. Harris, S. Andersen, B. Christiansen, N. Larsen, M. Rex, and B. Naujokat (2004), Extrapolating future arctic ozone loses, *Atmos. Chem. Phys.*, *4*, 1849–1856.

Kursinski, E. R., et al. (1996), Initial results of radio occultation observations of Earth's atmosphere using the global positioning system, *Science*, *271*, 1107–1110.

Kursinski, E. R., G. A. Hajj, J. T. Schofield, R. P. Linfield, and K. R. Hardy (1997), Observing Earth's atmosphere with radio occultation measurements using the global positioning system, *J. Geophys. Res.*, *102*, 23,429–23,465.

Kursinski, E. R., G. A. Hajj, S. S. Leroy, and B. Herman (2000), The GPS occultation technique, *Terr. Atmos. Oceanic Sci.*, *11*, 53–114.

Labitzke, K. (2005), On the solar cycle-QBO-relationship: A summary, *J. Atmos. Solar Terr. Phys.*, *67*, 45–54.

Lahoz, W. A., et al. (1994), Three-dimensional evolution of water vapour distributions in the Northern Hemisphere as observed by MLS, *J. Atmos. Sci.*, *51*, 2914–2930.

Larsen, N., et al. (2004), Formation of solid particles in synoptic-scale Arctic PSCs in early winter 2002/2003, *Atmos. Chem. Phys.*, *4*, 2001–2013.

Manney, G. L., J. L. Sabutis, S. Pawson, M. L. Santee, B. Naujokat, R. Swinbank, M. E. Gelman, and W. Ebisuzaki (2003), Lower stratospheric temperature differences between meteorological analyses in two cold Arctic winters and their impact on polar processing studies, *J. Geophys. Res.*, *108*(D5), 8328, doi:10.1029/2001JD001149.

Manney, G. L., K. Krüger, J. L. Sabutis, and S. A. Sena (2005), The remarkable 2003–2004 winter and other recent warm winters in the Arctic stratosphere since the late 1990s, *J. Geophys. Res.*, *110*, D04107, doi:10.1029/2004JD005367.

Montzka, S. A., et al. (2003), Scientific assessment of ozone depletion: 2002, *Rep. 47*, Global Ozone Res. and Monit. Project, World Meteorol. Org., Geneva, Switzerland.

Müller, M., R. Neuber, G. Beyerle, E. Kyrö, R. Kivi, and L. Wöste (2001), Non-uniform PSC occurrence within the Arctic polar vortex, *Geophys. Res. Lett.*, *28*, 4175–4178.

Namboothiri, S. P., J. Jiang, P. Kishore, K. Igarashi, C. Ao, and L. Romans (2008), CHAMP observations of global gravity wave fields in the troposphere and stratosphere, *J. Geophys. Res.*, *113*, D07102, doi:10.1029/2007JD008912.

Naujokat, B., K. Kruger, K. Matthes, J. Hoffmann, M. Kunze, and K. Labitzke (2002), The early major warming in December 2001 - exceptional?, *Geophys. Res. Lett.*, *29*(21), 2023, doi:10.1029/2002GL015316.

Preusse, P., S. D. Eckermann, and D. Offermann (2000), Comparison of global distributions of zonal-mean gravity wave variance inferred from different satellite instruments, *Geophys. Res. Lett.*, *27*, 3877–3880.

Randel, W. J., and F. Wu (1999), Cooling of the Arctic and Antarctic polar stratospheres due to ozone depletion, *J. Clim.*, *12*, 1467–1479.

Rex, M., et al. (2002), Chemical depletion of Arctic ozone in winter 1999/2000, *J. Geophys. Res.*, *107*(D20), 8276, doi:10.1029/2001JD000533.

Rex, M., R. J. Salawitch, P. von der Gathen, N. R. P. Harris, M. P. Chipperfield, and B. Naujokat (2004), Arctic ozone loss and climate change, *Geophys. Res. Lett.*, *31*, L04116, doi:10.1029/2003GL018844.

Rex, M., et al. (2006), Arctic winter 2005: Implications for stratospheric ozone loss and climate change, *Geophys. Res. Lett.*, *33*, L23808, doi:10.1029/2006GL026731.

Rocken, C., et al. (1997), Analysis and validation of GPS/MET data in the neutral atmosphere, *J. Geophys. Res.*, *102*, 29,849–29,866.

Schrøder, T. M., C. O. Ao, and M. de la Torre Juárez (2007), Sensitivity of GPS occultation retrieval to the stratopause, *J. Geophys. Res.*, *112*, D06119, doi:10.1029/2006JD007330.

Tabazadeh, A., R. P. Turco, K. Drdla, M. Z. Jacobson, and O. B. Toon (1994), A study of Type I polar stratospheric cloud formation, *Geophys. Res. Lett.*, *21*, 1619–1622.

Thayer, G. D. (1974), An improved equation for the radio refractive index of air, *Radio Sci.*, *9*, 803–807.

Tsuda, T., M. Nishida, C. Rocken, and R. H. Ware (2000), A global morphology of gravity wave activity in the stratosphere revealed by the GPS occultation data (GPS/MET), *J. Geophys. Res.*, *105*, 7257–7273.

Voigt, C., A. Tsias, A. Dörnbrack, S. Meilinger, B. Luo, J. Schreiner, N. Larsen, K. Mauersberger, and T. Peter (2000), Non-equilibrium compositions of liquid polar stratospheric clouds in gravity waves, *Geophys. Res. Lett.*, *27*, 3873–3876.

Wu, D., and F. Zhang (2004), A study of mesoscale gravity waves over North Atlantic with satellite observations and a mesoscale model, *J. Geophys. Res.*, *109*, D22104, doi:10.1029/2004JD005090.

M. de la Torre Juárez, G. A. Hajj, B. A. Iijima, A. J. Mannucci, S. Marcus, and T. M. Schrøder, Jet Propulsion Laboratory, California Institute of Technology, MS 169-237, 4800 Oak Grove Drive, Pasadena, CA 91189, USA. (mtj@jpl.nasa.gov)

A. Dörnbrack, Institut für Physik der Atmosphäre, DLR, D-82230 Oberpfaffenhofen, Germany.

R. Kivi, Arctic Research Centre, FMI, FI-99600 Sodankylä, Finland.